*Tellus* (1991), *43A*, 198–212

# The influence of interior gradients of potential vorticity on rapid cyclogenesis

By JOSEPH A. ZEHNDER[1] and DANIEL KEYSER[2], [1]*Institute of Atmospheric Physics, University of Arizona, Tucson, AZ 85721 USA*; [2]*Department of Atmospheric Science, State University of New York at Albany, Albany, NY 12222 USA*

(Manuscript received 29 January 1990; in final form 12 November 1990)

ABSTRACT

The evolution of cyclonic disturbances that are localized along the rigid upper and lower boundaries of a stratified, uniformly rotating, Boussinesq atmosphere is examined using an inviscid, adiabatic, two-dimensional, quasi-geostrophic model. The disturbances are characterized by either uniform or nonuniform potential vorticity. An imposed vertical shear of the geostrophic zonal wind provides the energy source for baroclinic development. The model simulations in this study are intended to address the possibility that a tropopause fold associated with an upper-level jet-front system overrunning a low-level air-mass boundary can result in rapid cyclogenesis, in the absence of diabatic effects. The interaction of baroclinically stable upper- and lower-level disturbances characterized by nonuniform potential vorticity results in a significant initial increase of the relative vorticity at the surface, in contrast to the decrease in relative vorticity exhibited by an isolated lower-level disturbance. The increase in relative vorticity associated with this rapid growth phase exceeds that predicted by normal-mode theory. Similar, but less pronounced, development occurs if the upper-level anomaly has nonuniform potential vorticity while the lower-level anomaly has uniform potential vorticity. Upper- and lower-level anomalies associated with uniform potential vorticity do not interact. Each disturbance behaves as a surface-trapped baroclinic wave. There is no increase in surface relative vorticity prior to the onset of the normal-mode growth phase. A diagnostic omega equation is presented, wherein the forcing is expressed equivalently as the advection of potential vorticity and perturbation vertical stratification by the thermal wind or as the advection of relative vorticity by the thermal wind. The omega equation is used to interpret the evolution of surface vorticity in terms of an induced vortex stretching for the various combinations of upper- and lower-level anomalies. When properly configured in the vertical, interior anomalies of potential vorticity are particularly conducive to surface development, with the primary cyclogenetic contribution due to advection of potential vorticity by the thermal wind. This forcing contribution dominates that related to perturbation stratification, which is shown to be cyclolytic. Alternatively, the vorticity fields associated with the upper- and lower-level potential vorticity anomalies overlap and reinforce each other, resulting in strong cyclogenetic forcing at lower levels through vorticity advection by the thermal wind. This study illustrates and clarifies some of the concepts associated with "potential-vorticity thinking" and the initial-value approach to baroclinic instability. It is suggested that nonuniform distributions of interior potential vorticity with realistic length and depth scales provide a forcing mechanism sufficient for the rapid development of localized surface cyclones.

## 1. Introduction

It is widely recognized that the available potential energy present in a baroclinic atmosphere is responsible for the growth of midlatitude wave disturbances. In a landmark contribution, Eady (1949) published a normal-mode stability analysis of a vertically sheared zonal flow. Eady's model provides an instability mechanism with growing disturbances that have a length scale and vertical structure in agreement with observations of midlatitude cyclones. For typical midlatitude values of the governing parameters, Eady's model predicts a maximum growth rate that corresponds to an e-folding time of about 1.2 days. Although this growth rate is not unrealistic, it is much smaller than that which occurs in cases of explosive cyclogenesis.

Observational studies suggest that mechanisms absent from Eady's model are important in the rapid development of surface cyclones. In particular, the interaction of finite-amplitude upper- and lower-level disturbances seems to be important in initiating rapid growth. For example, in a climatological study of explosive cyclogenesis, Sanders and Gyakum (1980) found that in a majority of cases the rapidly deepening surface low was located approximately 750 km downstream of a mobile 500 mb trough. Detailed diagnostic analyses of individual storm systems, such as the 1979 Presidents' Day cyclone (Uccellini et al., 1985) and the QE II storm (Uccellini, 1986), have also indicated the importance of migratory upper-level disturbances in explosive cyclogenesis. In a recent model-based diagnostic study, Whitaker et al. (1988) have linked the rapid development phase of the 1979 Presidents' Day cyclone to the merging of two distinct potential vorticity maxima. There is an upper-level maximum associated with a tropopause fold and a lower-level maximum associated with a coastal front. The interested reader is referred to the article by Hibbard et al. (1989) for a dramatic three-dimensional depiction of the interaction of these features using state-of-the-art graphical visualization techniques. Another graphical illustration of cyclogenesis viewed in terms of the interaction between upper- and lower-level potential vorticity structures is presented for several observed cases by Bleck (1990).

Recent theoretical studies have focused on the treatment of initial-value problems. Pedlosky (1964) indicates that a continuous spectrum of solutions, which is absent from Eady's model, is necessary for a complete representation of the development of arbitrary disturbances in a baroclinic flow. Interior gradients of potential vorticity are necessary for the existence of the continuous spectrum; only those perturbations characterized by uniform potential vorticity may be represented as a superposition of Eady normal modes. If only unstable Eady modes are possible (horizontal wavenumbers less than the cutoff value), the long-term development is dominated by these modes, and the continuous spectrum is not necessary to describe the asymptotic temporal behavior. On the other hand, if only stable Eady modes are possible (horizontal wavenumbers greater than the cutoff value), the continuous spectrum must be included to represent the asymptotic temporal behavior. In either case, the continuous spectrum may contribute to the initial development of the disturbances.

Further insight into the importance of the continuous spectrum in baroclinic development is provided by Farrell (1984). Farrell considered the development of an Eady edge wave and showed that for a plane-wave initial condition the complete solution consists of a stable wave plus a contribution associated with the continuous spectrum that approaches zero asymptotically after an initial period of growth. Farrell also considered the development of a horizontally localized plane wave with a wavelength shorter than the cutoff value determined from normal-mode theory. He showed that modes with an initial upshear tilt grow, whereas vertical (barotropic) modes do not. Farrell associated this development with the interaction of favorably configured upper- and lower-level disturbances characteristic of so-called "type B" cyclogenesis (Petterssen et al., 1962; Petterssen and Smebye, 1971). A qualitative description of the dynamical mechanisms important to this type of interaction is given by Hoskins et al. (1985, pp. 928–930). A quantitative examination of the "type B" cyclogenesis mechanism based on experiments with idealized two-level and multi-level linear models initialized with realistic upper- and lower-level disturbances is found in the study by Warrenfeltz and Elsberry (1989).

An important question involves determining the characteristic attributes of the upper- and lower-level disturbances that are responsible for rapid development. In this paper, we will examine quantitatively the role of interior gradients of potential vorticity in the rapid development of cyclones by comparing the development of disturbances with nonuniform potential vorticity with that of disturbances possessing distributions of relative vorticity and potential temperature that are as similar as possible, but with uniform potential vorticity. Hoskins et al. (1985, p. 910) indicate that disturbances characterized by nonuniform interior potential vorticity and by uniform boundary distributions of potential temperature, as well as disturbances characterized by uniform interior potential vorticity and by nonuniform boundary distributions of potential temperature, both exhibit realistic wind and temperature distributions. They further propose that real cyclones may be visualized as consisting of various superpositions of these idealized forms.

Section 2 introduces the governing equations and techniques used in solving the initial-value problem. Section 2 also contains a discussion of specialized forms of the quasi-geostrophic omega equation that are useful for interpreting the results of the initial-value problem. The development of isolated lower-level disturbances characterized by either uniform or nonuniform potential vorticity is discussed in Section 3. The interaction of upper- and lower-level disturbances characterized by either uniform or nonuniform potential vorticity is discussed in Section 4. Section 5 contains a summary of the important results of this study and points toward areas for future research.

## 2. The model

### 2.1. Governing equations

The model consists of a rotating, stratified, adiabatic, inviscid atmosphere described relative to a rotating Cartesian reference frame $(x, y, z)$ with constant Coriolis parameter, $f = 1 \times 10^{-4}\ \mathrm{s}^{-1}$. We make the Boussinesq approximation and require the buoyancy frequency of the basic state to be constant ($N_0 = 1 \times 10^{-2}\ \mathrm{s}^{-1}$). The atmosphere is bounded above and below by flat, rigid surfaces.

We assume quasi-geostrophic dynamics, and the disturbances are taken to be two-dimensional. The development is thus governed by the conservation of quasi-geostrophic potential vorticity,

$$\frac{\mathrm{d}q}{\mathrm{d}t} = 0, \tag{2.1}$$

where

$$q = \frac{\partial^2 \psi}{\partial x^2} + \frac{f^2}{N_0^2}\frac{\partial^2 \psi}{\partial z^2}, \tag{2.2}$$

$$\frac{\mathrm{d}}{\mathrm{d}t} = \frac{\partial}{\partial t} + u_g \frac{\partial}{\partial x} + v_g \frac{\partial}{\partial y}. \tag{2.3}$$

Here, $\psi$ is the geostrophic streamfunction, and the subscript g indicates wind components that are in geostrophic balance. Conservation of potential temperature requires

$$\frac{\mathrm{d}\theta}{\mathrm{d}t} + \frac{N_0^2 \theta_0}{g} w = 0, \tag{2.4}$$

where $w$ is the vertical velocity, $g$ is the acceleration due to gravity, and $\theta$ and $\theta_0$ are total and reference potential temperature, respectively.

We prescribe a basic-state zonal flow of the form $u_g = U_0 + \lambda z$, where $U_0 = -15\ \mathrm{m\,s^{-1}}$, and the shear parameter $\lambda = 3 \times 10^{-3}\ \mathrm{s}^{-1}$. This type of zonal flow results in upper-level disturbances being advected over lower-level ones, with the interaction arranged to occur in the vicinity of $x = 0$ in the computational domain. The addition of a uniform zonal flow to the standard Eady model atmosphere does not affect the development, since the governing equations are Galilean invariant.

The prescription of the zonal flow field and the uniform basic-state stratification requires that the streamfunction be of the form

$$\psi(x, y, z, t) = \Psi(y, z) + \psi'(x, z, t), \tag{2.5}$$

where

$$\Psi(y, z) = \frac{g}{f} z + \frac{N_0^2 z^2}{2f} - (U_0 + \lambda z)\, y \tag{2.6}$$

is the basic-state streamfunction, which satisfies the governing equations identically. The basic state has uniform potential vorticity, $\bar{q} = f$, as can be seen by substituting (2.6) into (2.2). The flow variables are related to the geostrophic streamfunction through

$$u_g = -\frac{\partial \Psi}{\partial y}, \qquad v_g = \frac{\partial \psi'}{\partial x}, \qquad \theta = \frac{f\theta_0}{g}\frac{\partial \psi}{\partial z}. \tag{2.7a, b, c}$$

A comment on the set of eqs. (2.1)–(2.7) is in order. The assumption of two-dimensionality requires that $\psi$ be a function of $x$ and $z$, except for a component which specifies the zonal wind, $u_g(z)$. This zonal wind component remains constant in time. Under these assumptions, the three-dimensional nonlinear quasi-geostrophic equations reduce to a two-dimensional linear set without any explicit linearization.

*2.2. Method of solution*

We seek a numerical solution of the initial-value problem posed by (2.1)–(2.4). The method of solution follows that described in Zehnder and Bannon (1988), where a geostrophic-momentum analogue of the present model is employed. We begin by specifying an initial geostrophic streamfunction. This provides initial distributions of wind, potential temperature and potential vorticity through (2.7a, b, c) and (2.2), respectively. Eq. (2.1) is used to determine numerically a new distribution of potential vorticity in the interior. Likewise, (2.4) provides new values of the potential temperature along the upper and lower boundaries, where $w=0$. The new potential vorticity distribution is used to determine the new geostrophic streamfunction through inverting (2.2), with the new values of $\theta$ providing a Neumann boundary condition on $\psi$ via (2.7c). Lateral Neumann boundary conditions on $\psi$ are obtained by numerically integrating the meridional momentum equation with the assumption that the ageostrophic zonal flow vanishes identically. The new streamfunction provides updated wind and potential temperature distributions, and the integration proceeds forward in time.

The length of the computational domain is 6000 km and the depth is 10 km. The finite-difference grid contains 121 points in the horizontal and 33 points in the vertical, yielding a horizontal resolution of 50 km and a vertical resolution of 313 m. Details of the numerical methods used for solving the diagnostic equation for the geostrophic streamfunction (2.2) and the prognostic equations (2.1) and (2.4) may be found in Zehnder and Bannon (1988).

*2.3. Diagnostic analysis*

In our two-dimensional quasi-geostrophic system, the time rate of change of relative vorticity is given by

$$\frac{\partial \zeta}{\partial t}+u_g\frac{\partial \zeta}{\partial x}=f\frac{\partial w}{\partial z}, \tag{2.8}$$

where $\zeta=\partial v_g/\partial x$ is the relative vorticity. Local changes in relative vorticity are possible only through its advection by the basic-state zonal flow and through stretching of planetary vorticity. In this study, we are interested in the development of the maximum relative vorticity at the surface. Since $\partial\zeta/\partial x$ equals zero where $\zeta$ is a local maximum, we may ignore changes in $\zeta$ due to advection and consider only vortex stretching.

The diagnostic analysis is based on specialized forms of the quasi-geostrophic omega equation applicable to the Eady model atmosphere:

$$\left(\frac{\partial^2}{\partial x^2}+\frac{f^2}{N_0^2}\frac{\partial^2}{\partial z^2}\right)w=\frac{2f}{N_0^2}\frac{\partial u_g}{\partial z}\frac{\partial q}{\partial x}-\frac{2gf^2}{\theta_0 N_0^4}\frac{\partial u_g}{\partial z}\frac{\partial^2\theta'}{\partial x\,\partial z}, \tag{2.9a}$$

$$\left(\frac{\partial^2}{\partial x^2}+\frac{f^2}{N_0^2}\frac{\partial^2}{\partial z^2}\right)w=\frac{2f}{N_0^2}\frac{\partial u_g}{\partial z}\frac{\partial^2 v_g}{\partial x^2}, \tag{2.9b}$$

where $\partial u_g/\partial z=\lambda$, and $\theta'$ is perturbation potential temperature [related hydrostatically to $\psi'$ through (2.7c)]. In (2.9a), the forcing is partitioned into terms representing the advection of potential vorticity and perturbation vertical stratification by the thermal wind. This is a two-dimensional Galilean invariant form of the forcing in the omega equation given by Hoskins et al. (1985, pp. 938–940), which partitions the vertical motion into contributions associated with the vertical shear of the advection of potential vorticity, boundary temperature advection, and isentropic upgliding. In (2.9b), the forcing consists of the advection of relative vorticity by the thermal wind. This form of the forcing is the two-dimensional counterpart of that introduced by Sutcliffe (1947) and discussed further by Hoskins et al. (1978), Trenberth (1978), and Hoskins and Pedder (1980).

The forcing term on the right-hand side of (2.9a) representing the advection of potential vorticity by the thermal wind contributes only if the potential vorticity is nonuniform. This component is associated with nonmodal development due to the continuous spectrum. The forcing term representing the advection of perturbation stratification by the thermal wind contributes for both uniform and nonuniform potential vorticity. In cases with uniform potential vorticity, this term is associated with modal development. Examination of the vortex stretching due to each component through (2.8) will provide a quantitative basis for describing and comparing the evolution of both isolated and interacting upper- and lower-level disturbances characterized by various combinations of uniform and nonuniform potential vorticity.

Several caveats should be pointed out regarding the form of the forcing in (2.9a). First, the individual forcing terms are subject to internal cancellation because the effect of perturbation stratification is included in both of them. Second, the forcing terms are not dynamically independent in the sense that, at any instant, the perturbation stratification is associated with both the interior distribution of potential vorticity and the boundary distribution of potential temperature. Thus, the partitioning in (2.9a) is purely diagnostic; it should not be thought of as isolating the dynamical effects of interior potential vorticity gradients and boundary potential temperature gradients in the same sense that the height tendency may be decomposed into the effects of potential vorticity advection in the interior and potential temperature advection at the upper and lower boundaries.* Nevertheless, the separation between these effects cannot be generalized in a prognostic sense, since the boundary potential temperature distribution evolves in response to meridional advection induced by the interior potential vorticity distribution in addition to that which is self-induced. Therefore, it does not appear possible to isolate the development associated with the continuous spectrum from that of the normal modes in cases characterized by interior gradients of potential vorticity.

## 3. Development of isolated lower-level disturbances

In this section, we examine the development of isolated lower-level disturbances with either uniform or nonuniform potential vorticity. As we eventually will diagnose the extent of interaction between upper- and lower-level disturbances through a comparison with the behavior of isolated disturbances, a detailed treatment of the latter is in order.

* A partitioning that would provide such a separation in the context of the omega equation is a split of the relative vorticity in (2.9b) into components associated with the interior distribution of potential vorticity and the boundary distribution of potential temperature. This alternative was suggested to us by a reviewer.

### 3.1. Uniform potential vorticity

We specify an initial perturbation with uniform potential vorticity by assuming a boundary potential temperature distribution of the form

$$\theta'(x, z=0) = \Delta\theta \exp\left[-\left(\frac{x-x_0}{L}\right)^2\right], \tag{3.1}$$

where $\Delta\theta$ is the amplitude of the perturbation potential temperature, $L$ is the horizontal length scale of the disturbance, and $x_0 = 1000$ km is the initial location of the disturbance. Lateral boundary conditions on $\psi$ are

$$\psi(x_\pm, z) = \frac{g}{f} z + \frac{N_0^2 z^2}{2f}, \tag{3.2}$$

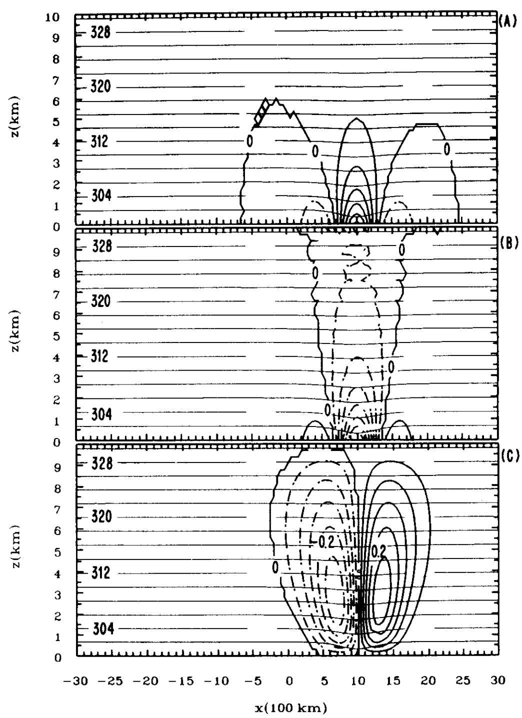


*Fig. 1.* Isopleths of potential temperature and (a) relative vorticity, (b) vertical perturbation potential temperature gradient, and (c) vertical velocity at $t=0$ for an isolated lower-level disturbance with uniform potential vorticity. Contour intervals are: 2 K for potential temperature (thin solid lines), $0.2 \times 10^{-5}$ s$^{-1}$ for relative vorticity, 0.05 K km$^{-1}$ for vertical potential temperature gradient, and 0.05 cm s$^{-1}$ for vertical velocity. For the latter fields, thick solid (dot-dashed) lines denote positive (negative) values.

where $x_+$ ($x_-$) represents the right (left) lateral boundary. Eq. (2.2) is solved subject to the boundary conditions (2.7c) and (3.2). The perturbation is assigned an amplitude $\Delta\theta = 1.2$ K and a length scale $L = 350$ km. This length scale is chosen so that the amplitudes of baroclinically unstable wave modes are initially small.

Fig. 1 shows the initial distributions of potential temperature, relative vorticity, perturbation stratification, and vertical velocity for the anomaly described above. A warm anomaly with uniform potential vorticity has a central region of positive (cyclonic) relative vorticity flanked by regions of anticyclonic relative vorticity (Fig. 1a). In order for the potential vorticity to be uniform, the perturbation stratification must be negative (positive) in regions of cyclonic (anticyclonic) relative vorticity (Fig. 1b).

Features of the vertical velocity field shown in Fig. 1c may be inferred by considering the signs of the forcing terms in (2.9a, b). In this case, only the stratification forcing term in (2.9a) contributes. The distribution depicted in Fig. 1b results in negative (positive) advection of perturbation stratification by the thermal wind and consequent cyclogenetic upward (cyclolytic downward) motion near the lower boundary on the downshear (upshear) side. Over a finite time interval, the vortex stretching associated with this vertical motion field results in a decrease (increase) of the anticyclonic relative vorticity on the downshear (upshear) side. The enhanced anticyclonic relative vorticity on the upshear side has associated with it a region of similarly enhanced positive perturbation stratification necessary for the conservation of potential vorticity, which leads to cyclolytic stretching in the region of maximum cyclonic relative vorticity. Similar reasoning regarding the advection of relative vorticity by the thermal wind (2.9b) can be applied to account for cyclolytic stretching and the eventual weakening of the cyclonic relative vorticity maximum.

A representation of the temporal evolution of the surface relative vorticity is depicted in Fig. 2. This plot corresponds to a Hovmöller diagram. The cyclonic relative vorticity maximum is located initially at $x = 1000$ km. The initial disturbance moves in the direction of the zonal flow at the surface, and the cyclonic relative vorticity maximum weakens and dissipates while the upshear anticyclonic relative vorticity maximum amplifies. This latter feature then weakens as a new upshear cyclonic relative vorticity maximum forms. This behavior is characteristic of an edge wave and results from the vortex-stretching mechanism outlined above. Support for this contention is found in

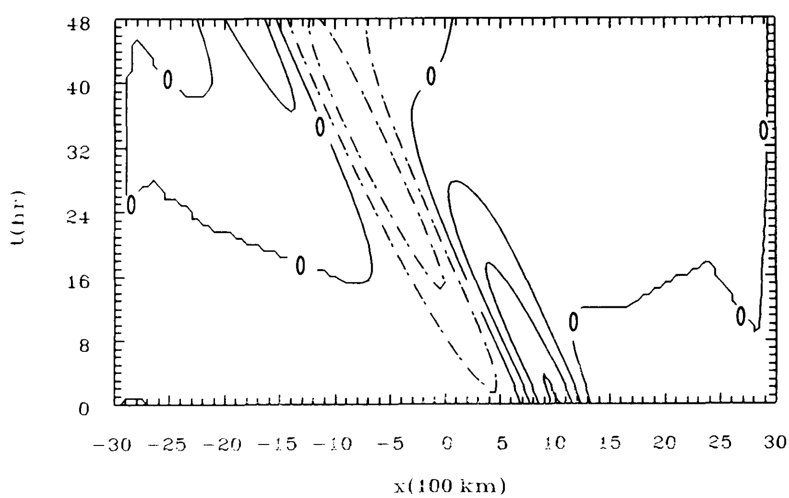


*Fig. 2.* Isopleths of surface relative vorticity for the isolated lower-level disturbance with uniform potential vorticity. The contour interval is $0.4 \times 10^{-5}$ s$^{-1}$.

the application of expressions for the phase and group velocity pertinent to a baroclinic edge wave (Gill, 1982; p. 552):

$$c_{\rm ph} = U_0 + \frac{f\lambda}{N_0 k}, \qquad c_{\rm gr} = U_0, \tag{3.3a, b}$$

where $k = 2\pi/l$ is horizontal wavenumber and $l$ horizontal wavelength. Taking $l$ to be 1200 km (twice the width of the region of surface cyclonic vorticity at $t = 0$; see Fig. 1a) yields $c_{\rm ph} = -9.3\ \mathrm{m\,s^{-1}}$, and $c_{\rm gr} = -15\ \mathrm{m\,s^{-1}}$. These values correspond closely to their counterparts determined graphically from Fig. 2, where $c_{\rm ph}$ is taken to correspond to the tracks of the axes of maximum and minimum relative vorticity ($\sim -1600$ km/48 h), and $c_{\rm gr}$ to the track defined by a line connecting the centers of maximum and minimum relative vorticity ($\sim -1650$ km/31 h).

### *3.2. Nonuniform potential vorticity*

We specify an initial perturbation with nonuniform potential vorticity by assuming a distribution of the form,

$$q'(x, z) = \Delta q \exp\left[-\left(\frac{x - x_0}{L}\right)^2 - \left(\frac{z}{H}\right)^2\right], \tag{3.4}$$

where $\Delta q$ ($=0.375f$) is the perturbation potential vorticity amplitude, and $L$ ($=350$ km) and $H$ ($=2$ km) are horizontal and vertical scales of the disturbance. We require that the potential temperature be uniform along the upper and lower boundaries. Thus, the initial disturbance is described completely by interior gradients of potential vorticity. Eq. (2.2) is solved for $\psi$, with the lateral boundary conditions given by (3.2). The parameters in (3.4) are chosen such that the maximum relative vorticity at the surface is the same as in the preceding case with uniform potential vorticity. Here, as in the preceding case, the initial amplitudes of baroclinically unstable wave modes are small.

Fig. 3 shows the potential temperature, potential vorticity, relative vorticity, perturbation stratification, and partitioned vertical velocity for the above-described anomaly. The effect of imposing a positive potential vorticity anomaly is to increase the vertical extent of the relative vorticity perturbation compared with the case of uniform potential vorticity (compare Fig. 3b with Fig. 1a). Both the relative vorticity and perturbation stratification are positive in the region of the potential vorticity anomaly; above the anomaly

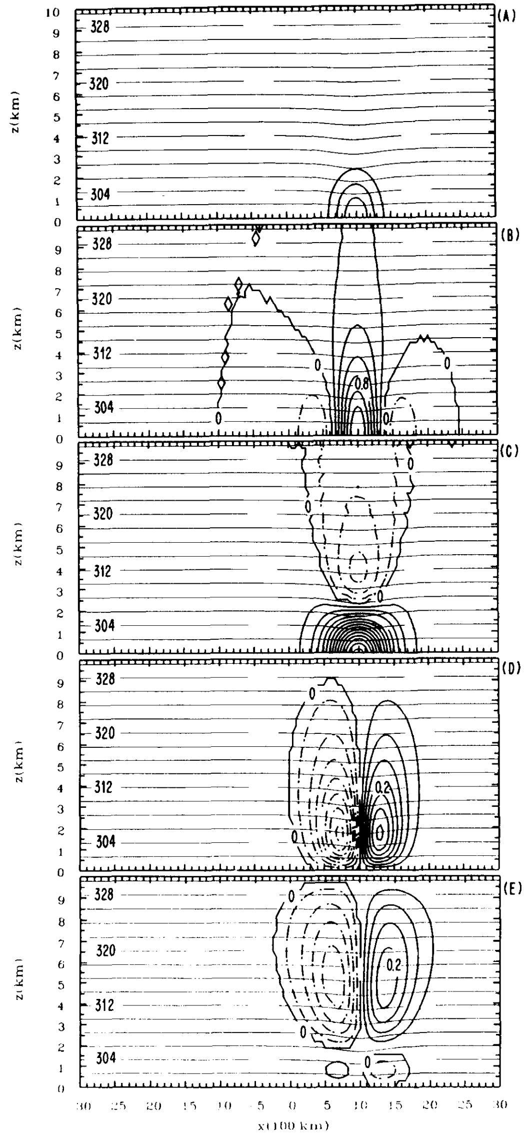


*Fig. 3.* Isopleths of potential temperature and (a) potential vorticity, (b) relative vorticity, (c) vertical perturbation potential temperature gradient, (d) vertical velocity forced by interior gradients of potential vorticity, and (e) vertical velocity forced by interior gradients of perturbation stratification at $t = 0$ for an isolated lower-level disturbance with nonuniform potential vorticity. Contour interval for potential vorticity is $0.1 \times 10^{-4}\ \mathrm{s^{-1}}$; other contour intervals are the same as in Fig. 1.

the perturbation stratification is negative (Fig. 3e). This configuration results in $\partial q/\partial x$ and $\partial^2\theta'/\partial x\, \partial z$ having the same sign at low levels. In this case, both forcing terms on the right-hand side of (2.9a) contribute to the vertical velocity. On the downshear side of the potential vorticity anomaly, $\partial q/\partial x < 0$. This results in positive advection of potential vorticity by the thermal wind and a contribution of cyclogenetic rising motion (Fig. 3d). The converse is true on the upshear side. On the downshear (upshear) side, there is positive (negative) advection of the perturbation stratification, resulting in a contribution of cyclolytic (cyclogenetic) stretching near the lower boundary (Fig. 3e).

A representation of the time evolution of the surface relative vorticity is depicted in Fig. 4. The initial relative vorticity maximum is located at $x = 1000$ km. Here, as in the preceding case, the disturbance exhibits edge wave behavior, with propagation in the direction of the surface zonal flow and a temporal oscillation of the sign of the maximum relative vorticity. Initially, the contributions of the potential vorticity and stratification terms agree with the above qualitative description, with the potential vorticity term dominant. The net vortex stretching leads to an initial decrease in the magnitude of the cyclonic relative vorticity maximum, and an increase in the magnitude of the upshear anticyclonic relative vorticity maximum. As in the preceding case, the increase in the anticyclonic relative vorticity maximum is associated with the generation of positive perturbation stratification, which results in cyclolytic stretching in the region of the cyclonic relative vorticity maximum. The corresponding interpretation involving vortex stretching induced by vorticity advection by the thermal wind derives from the development of an increasing downshear tilt to the potential vorticity and associated vorticity anomalies with time. As a result of this increased downshear tilt, the region of cyclolytic stretching that initially overlies the upshear anticyclonic relative vorticity maximum eventually overspreads the cyclonic relative vorticity maximum.

We have considered the development of two types of isolated lower-level disturbances. In each case, the disturbance is characterized by a warm temperature anomaly and cyclonic relative vorticity. The fundamental difference is the presence of interior gradients of potential vorticity in the latter case. Despite this difference, vortex stretching leads to a stable edge-wave behavior manifested by the absence of a long-term increase in the magnitude of the relative vorticity.

## 4. Development of upper- and lower-level disturbances

The interaction of cyclonic disturbances that are localized along the upper and lower boundaries is

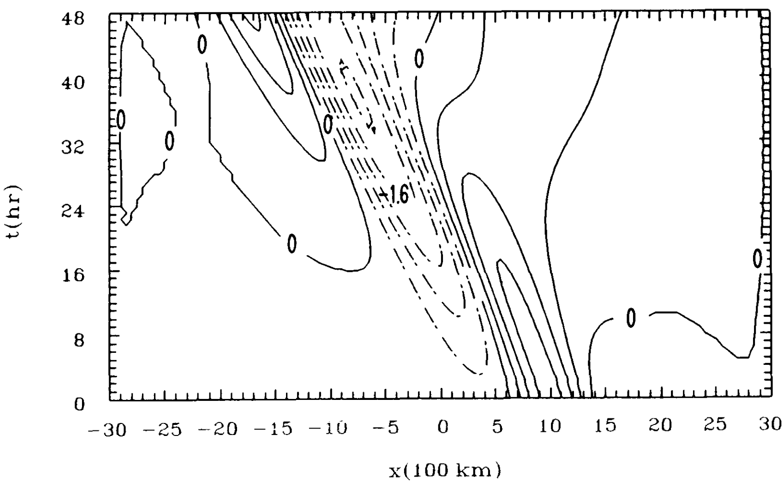


*Fig. 4.* Same as Fig. 2 for an isolated lower-level disturbance with nonuniform potential vorticity.

examined in this section. As in the preceding section, we will consider disturbances with uniform or nonuniform potential vorticity. We specify a potential vorticity distribution of the form

$$q'(x, z) = \Delta q \times \exp\left[-\left(\frac{x - x_0 - \sigma z}{L}\right)^2 - \left(\frac{z}{H}\right)^2\right]. \quad (4.1)$$

This expression is similar to (3.4), with the addition of a parameter $\sigma$ that defines the slope of the potential vorticity anomaly. A slope is imposed to provide an initial potential vorticity structure in agreement with observations of upper-level frontal zones (e.g., Keyser and Shapiro, 1986) and to ensure that the potential vorticity anomalies are aligned nearly vertically as they pass over each other under the action of the imposed zonal flow field. This configuration is consistent with observations (e.g., Boyle and Bosart, 1986). We assume that the potential temperature is initially uniform along the upper and lower boundaries.

The choice of perturbation potential vorticity parameters is motivated by the diagnostic observational and modeling studies of the Presidents' Day cyclone by Uccellini et al. (1985) and Whitaker et al. (1988), respectively. Upper-level potential vorticity anomalies result from intrusions of stratospheric air associated with tropopause folding, whereas the lower-level anomalies are due to boundary-layer processes or latent heat release (Whitaker et al., 1988). From observational considerations, it is reasonable to anticipate that the upper-level anomaly should be stronger and deeper than the lower-level one. When disturbances with uniform potential vorticity are considered later in this section, the boundary potential temperature distributions are of the form (3.1). In all cases considered, lateral boundary conditions are given by (3.2), and (2.2) is solved for geostrophic streamfunction.

Fig. 5 shows the initial distributions of potential temperature and potential vorticity for cases respectively consisting of upper- and lower-level interior potential vorticity anomalies with uniform boundary potential temperature, and boundary potential temperature anomalies with uniform interior potential vorticity. The distributions of relative vorticity and perturbation stratification may be inferred qualitatively from Figs. 1 and 3. In

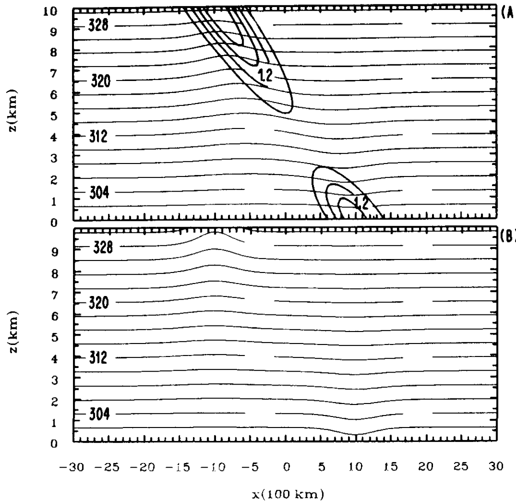


*Fig. 5.* Isopleths of (a) potential temperature and potential vorticity at $t = 0$ for upper- and lower-level disturbances with nonuniform potential vorticity, and (b) potential temperature at $t = 0$ for upper- and lower-level disturbances with uniform potential vorticity. Contour intervals are the same as in Fig. 3.

Fig. 5a, the upper-level anomaly has an amplitude $\Delta q = 0.5f$, a length scale $L = 350$ km, and a depth scale $H = 4$ km. The lower-level anomaly has $\Delta q = 0.375f$, $L = 350$ km, and $H = 2$ km, as in Subsect. 3.2. In Fig. 5b, the upper-level anomaly has amplitude $\Delta\theta = -2.2$ K, and the lower-level anomaly has $\Delta\theta = 1.2$ K, as in Subsect. 3.1. The length scale of both anomalies is $L = 350$ km. The perturbation potential temperature amplitudes are chosen so that the maximum relative vorticities at the upper and lower boundaries are the same for the disturbances with uniform and nonuniform potential vorticity. Here, as in Sect. 3, the length scale is chosen so that the initial amplitudes of baroclinically unstable wave modes are small. For the configuration in Fig. 5a, any initial increase in the relative vorticity may be attributed to the continuous spectrum of modes associated with interior gradients of potential vorticity, whereas for the configuration in Fig. 5b only the discrete spectrum of Eady modes is present.

The surface development of relative vorticity resulting from the case of upper- and lower-level disturbances with nonuniform potential vorticity is shown in Fig. 6a. There is a significant initial increase in the cyclonic relative vorticity at the sur-

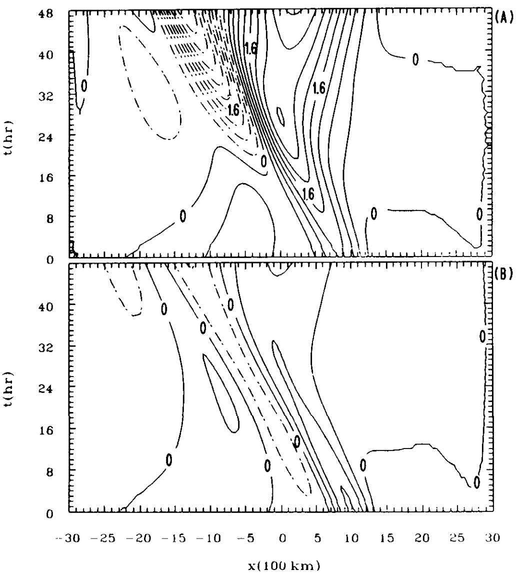


*Fig. 6.* Same as Fig. 2 for (a) upper- and lower-level disturbances with nonuniform potential vorticity, and (b) upper- and lower-level disturbances with uniform potential vorticity.

face, in contrast to the decreasing cyclonic relative vorticity of the isolated lower-level disturbance with nonuniform potential vorticity (Fig. 4). The time rate of change following the maximum of the normalized relative vorticity, $\delta \ln(\zeta/\zeta_0)/\delta t$, associated with this rapid development phase indicates a growth rate of about 1 day$^{-1}$ compared with 0.8 day$^{-1}$ for the fastest growing Eady normal mode. The maximum rate of vorticity increase occurs when the upper-level disturbance is slightly upstream of the lower-level one. Subsequently, the upper- and lower-level disturbances are advected past each other, resulting in a period of weak cyclolysis. After a sufficient interval the baroclinically unstable modes become dominant. The normal-mode growth phase begins at $t \sim 37$ h.

The surface development resulting in the case of upper- and lower-level disturbances characterized by uniform interior potential vorticity is shown in Fig. 6b. Here the upper- and lower-level anomalies do not appear to interact, with each disturbance behaving as a baroclinic edge wave. There is no apparent increase in the cyclonic relative vorticity at the surface prior to the onset of the normal-mode growth phase. The dynamical mechanisms responsible for the interaction of the disturbances in the first case and the apparent lack of interaction in the second case are examined by considering the partitioned vortex stretching given by (2.9a).

Fig. 7a shows the maximum cyclonic relative vorticity at the surface, along with the individual and total vortex-stretching contributions evaluated at the location of the vorticity maximum, as a function of time for the first case. If we consider the first 28 h of development, we see that the potential vorticity component is cyclogenetic, whereas the stratification component is cyclolytic, with the former having the larger magnitude. The signs of the vortex stretching terms associated with each forcing component are consistent with the qualitative interpretations developed in Sect. 3. The dominance of the potential vorticity term results in the increase in relative vorticity during this period. The maximum growth rate occurs at $t = 17$ h, slightly before the potential vorticity component attains a maximum. This indicates that although the potential vorticity term is cyclogenetic the details of the development depend on the thermal structure of the low-level perturbation through the stratification term. The cyclogenetic contribution of the upper-level potential vorticity anomaly at low levels acts to suppress the development of the upshear anticyclonic relative vorticity maximum and the concomitant increase in perturbation stratification, and the potential vorticity term remains dominant through this period.

Between 28 and 35 h, the signs of the potential vorticity and stratification terms are the same as during the first 28 h, but now the stratification term has the larger magnitude. This leads to a decrease in the cyclonic relative vorticity during this period. After 36 h, the potential vorticity term rapidly approaches zero and the stratification term becomes cyclogenetic. This behavior signifies the development of the Eady normal modes.

Fig. 7b shows the maximum cyclonic relative vorticity at the surface and the stretching terms at this maximum for the upper- and lower-level disturbance characterized by uniform potential vorticity. In this case, the stretching due to potential vorticity is zero, and the development is governed by the stratification term. During the first 22 h of development, the stratification term is cyclolytic and results in a decrease of relative vorticity. The stratification term is cyclogenetic between 22 and

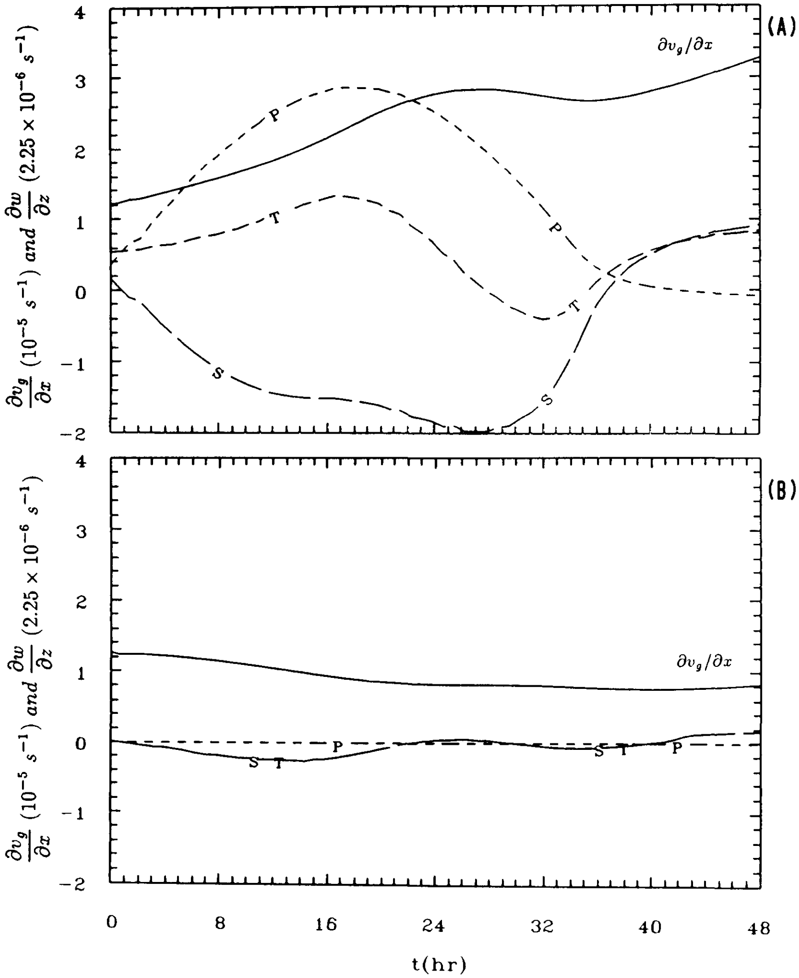


*Fig. 7.* Plots of the maximum cyclonic relative vorticity (solid line) and the partitioned vortex stretching normalized by $f$ due to the potential vorticity ($P$) and the stratification ($S$), along with the total ($T$), at the position of the surface vorticity maximum as a function of time for the initial states described in Fig. 5. The units of relative vorticity and normalized vortex stretching, $\partial w/\partial z$, are $10^{-5}$ $s^{-1}$ and $2.25 \times 10^{-6}$ $s^{-1}$, respectively.

30 h, suggesting some form of weak interaction between the upper- and lower-level disturbances. The cyclogenetic tendency is small relative to that in the preceding case and results in a negligible increase in cyclonic relative vorticity during this period. The relative weakness of the interaction is due to the shallowness of the respective vertical circulations associated with the upper- and lower-level anomalies compared with the preceding case. After 39 h, the stratification term becomes cyclogenetic and the cyclonic relative vorticity begins to increase. This transition marks the onset of the normal-mode growth phase.

Additional insight into the interaction of upper- and lower-level disturbances is obtained by considering the development of an upper-level disturbance with nonuniform potential vorticity and a lower-level disturbance with uniform potential vorticity. The upper-level anomaly has the same amplitude, length, and depth scales as the upper-level anomaly in Fig. 5a, whereas the lower-level anomaly has the same parameter values as the

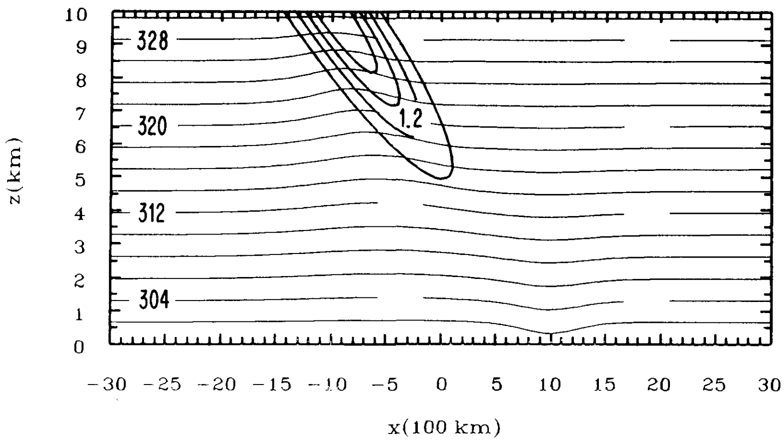


*Fig. 8.* Isopleths of potential temperature and potential vorticity for an upper-level disturbance with nonuniform potential vorticity and a lower-level disturbance with uniform potential vorticity. Contour intervals are the same as in Fig. 3.

lower-level anomaly in Fig. 5b. The initial distributions of potential temperature and potential vorticity for this "hybrid" case are shown in Fig. 8. Surface development in terms of relative vorticity is portrayed in Fig. 9. The qualitative features of the development are similar to those in Fig. 6a. The rapid development phase begins later, however, and the maximum growth rate is smaller (0.78 $\text{day}^{-1}$ compared with 1 $\text{day}^{-1}$), resulting in smaller values of the maximum cyclonic relative vorticity. Consideration of the partitioned vortex stretching (not shown) reveals that the weaker cyclogenesis compared with the case shown in Fig. 7a is related to a substantially reduced cyclogenetic contribution at the lower boundary associated with potential vorticity forcing. This reduction is due to the absence of potential vorticity gradients near the lower boundary. The stratification term is cyclolytic during the early stages of the development, but the magnitude of this cyclolytic contribution diminishes with time, resulting in a total stretching contribution qualitatively similar to that shown in Fig. 7a.

Examination of (2.9a) indicates that the relative

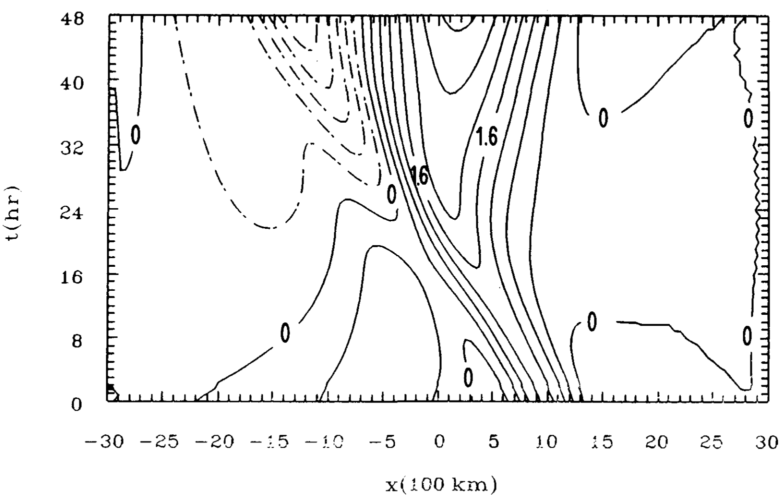


*Fig. 9.* Same as in Fig. 2 for the initial state described in Fig. 8.

contributions of the potential vorticity and stratification forcing terms may be altered by varying the value of the background stratification, $N_0$. For relatively small values of $N_0$, the stratification term will become dominant. A number of model runs were performed with disturbances such as those in Figs. 5a, b and values of $N_0$ ranging between $0.9 \times 10^{-2}\,\mathrm{s}^{-1}$ and $0.5 \times 10^{-2}\,\mathrm{s}^{-1}$. In these cases, the normal mode development was evident earlier in the model runs. This behavior is consistent with a decrease in the cutoff wavelength for instability. Since the cutoff wavelength decreases with $N_0$, the spectrum of baroclinically unstable components in the initial disturbance increases, favoring normal-mode growth. Alternatively, decreased $N_0$ results in an increased vertical penetration scale (Rossby depth) of the upper- and lower-level disturbances, leading to sufficient overlap of the disturbances to facilitate normal-mode growth.

The results of this study should not be taken to suggest that baroclinically stable structures with nonuniform potential vorticity are the only structures that support growth. It is possible for baroclinically stable disturbances with uniform potential vorticity to exhibit an increase in amplitude. Consider, for example, two neutral baroclinic edge waves based at the lower boundary, each having amplitude $A_0$ but slightly differing zonal wavenumbers. If the waves are initially 180° out of phase, superposition results in zero amplitude in a localized region. Since the phase speed depends on the Rossby depth and hence the wavenumber, after some time the waves will be in phase, resulting in a total wave amplitude of $2A_0$. This flow configuration appears to be too restrictive to be realized in the atmosphere*.

A more realistic model of the growth of baroclinically stable structures is investigated by Rotunno and Fantini (1989). They consider the interaction of neutral Eady modes respectively associated with the upper and lower boundaries. The interaction is capable of extracting perturbation kinetic energy from the basic-state flow. This indicates that the growth identified in their model is not simply due to superposition, which explains the growth in the previous example. In identifying a cyclogenetic interaction between neutral Eady modes in the absence of structures associated with interior gradients of potential vorticity (continuous-spectrum effects), Rotunno and Fantini (1989) complement the results of the present study and Farrell (1984). Rotunno and Fantini's model corresponds to the configuration exhibited in Fig. 5b of the present paper, with the exception that the characteristic horizontal scale ($l/2\pi$) and Rossby depth ($fl/2\pi N_0$) of the upper- and lower-level disturbances are large enough ($\sim 350$ km and $\sim 3.5$ km, $N_0$ and $f$ the same as in our study) to facilitate overlap and interaction in the vertical, yet small enough to be baroclinically stable. Our approach consists of studying the evolution of horizontally localized, rather than wavelike, upper- and lower-level disturbances, with horizontal scales characteristic of observations of rapid cyclogenesis. The relatively small values of these scales ($l/2\pi \sim 191$ km, associated Rossby depth $\sim 1.9$ km; refer to edge-wave discussion in Section 3.1 for determination of $l$) suggests the necessity of interior gradients of potential vorticity to "extend" the disturbances sufficiently in the vertical to allow for cyclogenetic interactions between upper and lower levels (recall the relative vorticity fields in Figs. 1a and 3b).

## 5. Summary

This study focuses on some of the concepts associated with "potential vorticity thinking" and the initial-value approach to baroclinic instability (Pedlosky, 1964; Farrell, 1984). Here, we have demonstrated that interacting upper- and lower-level disturbances with a particular structure (i.e., nonuniform interior potential vorticity) may undergo rapid growth.

* A plausible demonstration of cyclogenesis resulting from the evolution of a localized disturbance characterized by uniform potential vorticity is found in the study by Müller et al. (1989), which considers the evolution of a localized packet of stable normal modes in a *semi-geostrophic* framework. Cyclonic development is attributed not only to constructive interference of individual modes, but also to nonlinear interactions between them. The latter class of interactions is precluded from the model used in our study because it is linear, a consequence of the formulation of the two-dimensional Eady problem within a quasi-geostrophic framework (refer to the concluding paragraph of Subsect. 2.1).

The present work extends Farrell's (1984) study of the behavior of modal and non-modal baroclinic waves. By considering variations in the initial tilt and hence the initial thermal structure of horizontally localized, baroclinically stable structures, Farrell showed that modes with upshear tilt grow, whereas upright modes do not. Here, we examine the development of upper- and lower-level disturbances that are characterized by either uniform or nonuniform potential vorticity, but with similar interior distributions of potential temperature and relative vorticity. A comparison of the resulting growth rates exhibited by these disturbances shows that interior gradients of potential vorticity are conducive to the rapid initial growth of baroclinically stable structures.

We examine the effect of interaction between upper- and lower-level disturbances on surface cyclogenesis through comparison with surface development associated with isolated lower-level disturbances. Isolated lower-level disturbances characterized by uniform or nonuniform potential vorticity exhibit stable edge-wave behavior with an initial decrease in cyclonic relative vorticity and an increase in anticyclonic relative vorticity on the upshear side. In contrast, there is a significant increase initially in the relative vorticity at the surface when both the upper- and lower-level disturbances have nonuniform potential vorticity. The increase in surface vorticity is due to cyclogenetic vortex stretching that can be related to vertical motion forced by the advection of potential vorticity by the thermal wind. This cyclogenetic stretching is absent when the potential vorticity is uniform.

The differences in behavior of localized disturbances respectively characterized by uniform and nonuniform potential vorticity may be understood as follows: If the potential vorticity is uniform, then the depth of the disturbance is determined by its horizontal length scale through the Rossby depth. If the potential vorticity is nonuniform, then the depth of the disturbance is determined by the distribution of potential vorticity. Our results suggest that upper- and lower-level disturbances characterized by uniform potential vorticity and realistic length scales for observed cyclogenesis are too shallow to interact. In contrast, upper- and lower-level disturbance characterized by nonuniform potential vorticity, a length scale identical to that in the uniform case, realistic depth scales, and amplitudes yielding the same surface vorticity as in the uniform case are deep enough to interact, leading to robust surface cyclogenesis. In summary, the model results indicate that deep horizontally localized disturbances possessing realistic horizontal length scales grow, whereas their shallow counterparts do not, and that the depth of the growing disturbances is associated with nonuniformities in potential vorticity.

A deficiency of the quasi-geostrophic formulation adopted for this study is the neglect of advection by perturbation-induced velocities. Furthermore, quasi-geostrophic theory requires weak perturbations ($|\partial v_g/\partial x| \ll f$). The opportunity exists to extend the present work by examining the interaction of cyclonic disturbances using the two-dimensional geostrophic-momentum (GM) model described in Zehnder and Bannon (1988), but without topography. The assumptions inherent in the GM equations yield a dynamical system that better represents the mesoscale length scales considered in the present study. As a consequence of including advection by the ageostrophic circulation (the horizontal ageostrophic flow and the vertical velocity), the GM equations are expected to allow for higher-order interactions. For example, the ageostrophic zonal flow induced by perturbations such as those described in Section 4 is in the $-x(+x)$ direction at the top (bottom) of the model atmosphere; i.e., it opposes the geostrophic zonal flow. Thus, the ageostrophic zonal flow may act locally to slow the upper- and lower-level disturbances as they pass each other, increasing the length of time during which they can interact. Provided that the ageostrophic zonal flow at the top and bottom of the model atmosphere is associated respectively with descent and ascent in the interior, it is plausible that the vertical advection of potential vorticity will reduce the vertical separation between the upper- and lower-level anomalies, thus enhancing their dynamical interaction. If the ageostrophic circulation is sufficiently strong, the upper- and lower-level disturbances may (appealing to synoptic jargon) "phase" and "capture" each other. This would be expected to result in substantially larger growth rates than found in the quasi-geostrophic regime. These speculations may be addressed by considering the interaction of stronger ($\partial v_g/\partial x \geqslant f$) disturbances than are allowed in the quasi-geostrophic equations.

There is little doubt that diabatic processes also play an important role in explosive cyclogenesis. The opportunity exists to incorporate diabatic processes in the form of sensible and latent heating into the GM model. This would introduce an additional mechanism for forcing vertical motion and a means for generating interior gradients of potential vorticity. The treatment of diabatic effects would allow examination of the relative contribution of dynamics and thermodynamics to the rapid development of midlatitude cyclones.

## 6. Acknowledgments

This work was initiated while the authors were affiliated with the Severe Storms Branch of the Laboratory for Atmospheres, NASA/Goddard Space Flight Center, where JAZ held a NASA/NRC postdoctoral fellowship. DK acknowledges support through NSF Grant ATM-8721478 and ONR Contract N00014-88-K-0074 at the State University of New York at Albany. The authors have benefited from discussions with Drs. B. F. Farrell, R. Rotunno, and L. W. Uccellini.

REFERENCES

Bleck, R. 1990. Depiction of upper/lower vortex interaction associated with extratropical cyclogenesis. *Mon. Wea. Rev. 118*, 573–585.

Boyle, J. S. and Bosart, L. F. 1986. Cyclone-anticyclone couplets over North America. Part II: Analysis of a major cyclone event over the eastern United States. *Mon. Wea. Rev. 114*, 2432–2465.

Eady, E. T. 1949. Long waves and cyclone waves. *Tellus 1*, 33–52.

Farrell, B. 1984. Modal and non-modal baroclinic waves. *J. Atmos. Sci. 41*, 668–673.

Gill, A. E. 1982. *Atmosphere-ocean dynamics*. Academic Press, 662 pp.

Hibbard, W., Uccellini, L., Santek, D. and Brill, K. 1989. Application of the 4-D McIDAS to a model diagnostic study of the Presidents' Day cyclone. *Bull. Amer. Meteor. Soc. 70*, 1394–1403.

Hoskins, B. J. and Pedder, M. A. 1980. The diagnosis of middle latitude synoptic development. *Quart. J. Roy. Meteor. Soc. 106*, 707–719.

Hoskins, B. J., Draghici, I. and Davies, H. C. 1978. A new look at the $\omega$-equation. *Quart. J. Roy. Meteor. Soc. 104*, 31–38.

Hoskins, B. J., McIntyre, M. E. and Robertson, A. W. 1985. On the use and significance of isentropic potential vorticity maps. *Quart. J. Roy. Meteor. Soc. 111*, 877–946.

Keyser, D. and Shapiro, M. A. 1986. A review of the structure and dynamics of upper-level frontal zones. *Mon. Wea. Rev. 114*, 452–499.

Müller, J. C., Davies, H. C. and Schär, C. 1989. An unsung mechanism for frontogenesis and cyclogenesis. *J. Atmos. Sci. 46*, 3664–3672.

Pedlosky, J. 1964. An initial value problem in the theory of baroclinic instability. *Tellus 16*, 12–17.

Petterssen, S., Bradbury, D. L. and Pedersen, K. 1962. The Norwegian cyclone models in relation to heat and cold sources. *Geofys. Publ. 24*, 243–280.

Petterssen, S. and Smebye, S. J. 1971. On the development of extratropical cyclones. *Quart. J. Roy. Meteor. Soc. 97*, 457–482.

Rotunno, R. and Fantini, M. 1989. Petterssen's "type B" cyclogenesis in terms of discrete, neutral Eady modes. *J. Atmos. Sci. 46*, 3599–3604.

Sanders, F. and Gyakum, J. R. 1980. Synoptic-dynamic climatology of the "bomb." *Mon. Wea. Rev. 108*, 1589–1600.

Sutcliffe, R. C. 1947. A contribution to the problem of development. *Quart. J. Roy. Meteor. Soc. 73*, 370–383.

Trenberth, K. E. 1978. On the interpretation of the diagnostic quasi-geostrophic omega equation. *Mon. Wea. Rev. 106*, 131–137.

Uccellini, L. W. 1986. The possible influence of upstream upper-level baroclinic processes on the development of the QE II storm. *Mon. Wea. Rev. 114*, 1019–1027.

Uccellini, L. W., Keyser, D., Brill, K. F. and Wash, C. H. 1985. The Presidents' Day cyclone of 18–19 February 1979: Influence of upstream trough amplification and associated tropopause folding on rapid cyclogenesis. *Mon. Wea. Rev. 113*, 962–988.

Warrenfeltz, L. L. and Elsberry, R. L. 1989. Superposition effects in rapid cyclogenesis - Linear model studies. *J. Atmos. Sci. 46*, 789–802.

Whitaker, J. S., Uccellini, L. W. and Brill, K. F. 1988. A model-based diagnostic study of the rapid development phase of the Presidents' Day cyclone. *Mon. Wea. Rev. 116*, 2337–2365.

Zehnder, J. A. and Bannon, P. R. 1988. Frontogenesis over a mountain ridge. *J. Atmos. Sci. 45*, 628–644.